

DEVELOPMENT OF DEFORMABLE MODEL FOR 3D NONRIGID BREAST IMAGE REGISTRATION FOR IMPROVED BREAST CANCER DIAGNOSIS

Edward D. Lipson^{3,1,2}, Andrzej Krol^{1,2,3}, Mehmet Z. Unlu², Ioana L. Coman^{4,1,2}, James A. Mandef, Wei Lee¹, David H. Feiglin¹

¹Department of Radiology, SUNY Upstate Medical University

²Department of Electrical Engineering and Computer Science, Syracuse University

³Department of Physics, Syracuse University

⁴Department of Mathematics and Computer Science, Ithaca College

⁵Department of Civil and Environmental Engineering, Syracuse University

E-mail: edlipson@syr.edu

ABSTRACT

We have developed a finite element method (FEM) deformable breast model that does not require elastic breast data, and have applied it to nonrigid breast image registration a) for fusion of physiological (PET) and anatomical (MRI) images, and b) to correct for motion artifacts in dynamic MRI and PET breast scans. The model is applicable only if the stress conditions in the imaged breast are virtually the same in PET and MRI. Under these conditions, the observed displacements between PET and MRI are due to differences in the imaging/reconstruction process. Sufficiently similar stress conditions between the two modalities are assured by use of the MRI breast-antenna replica for breast support during PET and by the same positioning. Tetrahedral volume elements and triangular surface elements are used to construct the FEM mesh from an MRI image. Our model requires a number of fiducial skin markers (FSM) visible in both PET and MRI. After the displacement vectors of FSM are measured, the dense displacement field is estimated by distributing the displacement vectors linearly over the breast surface, and then throughout the volume. Finally, the floating MRI image is warped and fused with a fixed PET image using an appropriate shape function in the interpolation from mesh nodes to voxels. For motion correction in a dynamic scan series, the floating, post-injection image is warped to the fixed, pre-injection image. We tested our model on a small number of patients imaged with FSM using PET and MRI. For lesions visible in both PET and MRI, we established that the target registration error (TRE) is less than the width of two PET voxels for intermodal coregistration, and two MRI voxels for MRI dynamic sequence. Subtraction of the motion-corrected post-injection images from the pre-injection image revealed the true spatial distribution of the contrast material.

INTRODUCTION

Among women in the United States, breast cancer is the most common malignant disease and the second leading cause of cancer death [1]. Major goals in breast cancer diagnosis include early detection and characterization. The main tool for detection and diagnosis of breast cancer is x-ray mammography. The normal follow-up diagnostic treatment following an equivocal or difficult-to-interpret screening mammography is surgical biopsy. Since the majority of breast biopsies are negative [2], it would be highly desirable to have an alternative, noninvasive approach as the second line of defense after mammography. For further differentiation, other non-invasive imaging modalities, i.e. PET and MRI, can be used. We have investigated a 3D finite-element model (FEM) based deformable breast model for intermodality (PET and MRI) nonrigid breast-

image co-registration. This model estimates the displacement field for any location in the breast from the observed displacements of external fiducial markers visible in both PET and MRI.

MATERIALS AND METHODS

Phantom Studies. For our experiments, we used a custom-manufactured deformable breast phantom (CIRS Inc., Norfolk, VA; www.cirsinc.com), filled with medium-stiffness gel (vinyl-based hydrolymer with low concentration of nickel chloride) and surrounded by a skin made of thin urethane foil (Fig. 1).

The phantom was imaged using F-18 FDG positron emission tomography (PET) and high-resolution magnetic resonance imaging (MRI); for scan details, see Table 1.

Breast "lesions" visible in MRI were emulated by injection of oil (Johnson &

Johnson) non-diffusing in the gel containing a mixture of organic azo dyes. F-18-FDG, diluted in water-soluble gelatin with organic dyes, was injected as close as possible to the “lesions” that emulated lesions visible in PET. Six internal “lesions” could be uniquely identified in both PET and MRI (Fig. 2).

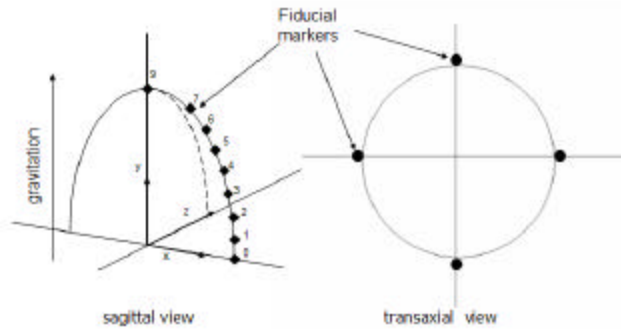


Fig. 1. Elastic breast phantom with external fiducial markers. Eight markers are placed on each four meridians, and one additional marker is placed on the apex.

Table (1). Imaging specifications.

	MRI	PET
Scanner	Philips 1.5 T, Intera	GE Advance
Scan Parameters	T1-weighted isotropic 3D FFE sequences with flip angle 20°	Transmission scan 3 min Emission scan 5 min
Spatial Resolution	0.7 mm	<7 mm
Acquisition/Reconstruction matrix	512 × 512	128 × 128
Voxel size (mm)	0.7 × 0.7 × 1.12	4.25 × 4.25 × 4.25

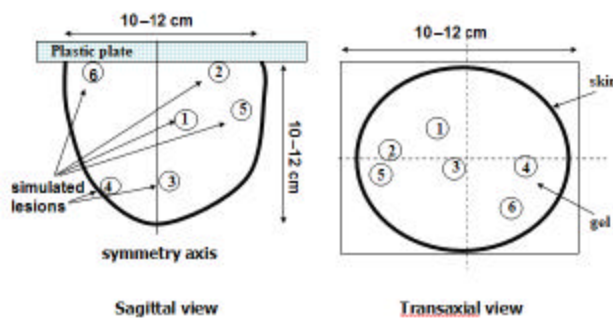


Fig. 2. Location of “lesions” inside elastic breast phantom.

Int. J. Sci. Res., vol. 15 (2002), pp. 8-1.

A deformable, finite-element method (FEM) based model of the elastic breast phantom was constructed [3,4]. We assumed that stress conditions within the phantom were virtually the same for both modalities. This is justified, because the phantom was leveled and freely suspended in PET and MRI.

The analogy between orthogonal components of the displacement field and the temperature differences in steady-state heat transfer (SSHT) in solids was adopted for our deformable FEM-based breast model. The model allows estimation of the intermodal breast deformation for every location within the breast from observed intermodal displacement of fiducial skin markers that are considered the FEM “loads”. The displacement field components u_x , u_y , u_z are mathematically equivalent to temperature differences in the steady-state heat transfer problem and are all distributed linearly over the phantom domain. Figure 3 shows images of fiducial markers and “lesions” in the elastic breast phantom obtained using PET and MRI.

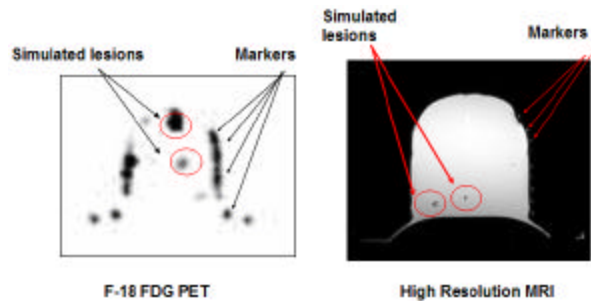


Fig. 3. Representative placement of “lesions” inside deformable breast phantom.

The geometry of the breast was obtained from MRI; meshing and analysis were performed using the commercial software ANSYS¹. The following elements were chosen from the ANSYS library: a) *SOLID87* 3D 10-Node Tetrahedral Thermal Solid; b) *SOLID70* 3D Thermal Solid; and c) *SHELL57* 2D Thermal Shell. A mesh containing a total of 15,636 nodes was created. *SOLID87* and *SOLID70* elements were used in the bulk interior of the object. The surface was meshed by a layer of *SHELL57* elements. The mesh used is shown in Fig. 4.

¹ANSYS, ver. 5.7 (ANSYS Inc., Canonsburg, PA)

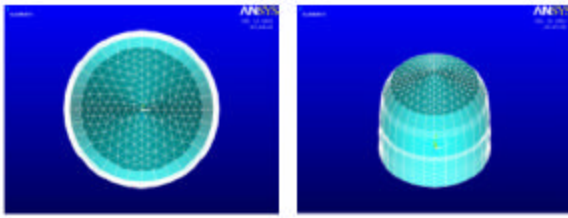


Fig. 4. FEM mesh generated by ANSYS software. *Left:* top view. The outer ring (white) shows shell elements. The inner ring shows brick elements. The central (and uppermost) area has tetrahedral elements. *Right:* oblique view. Brick elements are visible on the sides, and tetrahedral elements at and near the top

Thermal conductivity assigned to these surface elements was 1,000 times that used in the bulk of the phantom to ensure that the surface layer reaches steady state 1,000 times faster than the interior. Intermodal displacements (between PET and MRI) for every location within the phantom were obtained. The execution time was 20 s per Cartesian component for the entire mesh using a 3 GHz, dual Xeon processor PC.

Patient Studies.

We acquired PET and MRI data with fiducial skin markers on a few patients and applied our SSHT FEM coregistration technique to perform the multimodal PET/MRI and intramodal MRI/MRI image coregistration in 3D. The MRI scans were performed using a 1.5 T Philips Intera scanner. The PET scans were performed on a GE Discovery ST PET/CT system that combines a BGO PET scanner with a 4-slice CT scanner and is capable of 2D, 3D and 4D imaging. The high resolution MRI scan currently obtained for anatomical purpose also works very well for defining the surface of the breast. This 3D T1 weighted sequence has been obtained without fat saturation, so that the skin surface is easily visualized. The signal arising from skin is 16 times the noisy background observed in the vicinity of the breast. Voxels, having an edge dimension of 1.2 mm, were obtained with nearly isotropic resolution. These factors permit automated computer segmentation via simple thresholding with good definition of the breast surface. Similarly, in images obtained in the dynamic GRE MRI acquisition

series, breast skin is well defined and can be easily segmented out via thresholding. Segmented breast surface was used to create the FEM mesh with the ANSYS package. The geometric centroids of fiducial markers visible in PET and MRI were estimated using an iterative method, and the discrete displacement field was obtained. These data allowed our FEM model to obtain a dense displacement field (i.e. a displacement vector for each mesh node), which in turn was used to warp, in 3D, the moving MRI image to the target PET image or to warp the post-contrast MRI image to the pre-contrast MRI image, to obtain MRI differential dynamic series images. Coregistered images were fused using the Analyze software package.

RESULTS

Phantom Studies

We estimated two categories of errors: fiducial marker-registration error (FRE), and target-registration error (TRE); see Table 2 and Fig. 5. FRE was estimated for the fiducial markers that were excluded from the registration process, while TRE was estimated for the internal “lesions”. We have established that intermodal elastic breast phantom coregistration performed using our SSHT deformable breast model with external fiducial markers is accurate to within ~5mm (voxel size in PET). The TRE can be as large as two PET voxels, if proximal fiducial markers do not surround the “lesion”.

Table (2). Fiducial registration errors¹.

No. of markers used in FEM model	Mean Error (mm)	Standard Deviation (mm)	Min Error (mm)	Max Error (mm)
13	4.06	1.55	2.32	9.94
8	4.27	2.16	1.55	1.55
27 (all)	7×10^{-5}	8×10^{-5}	2×10^{-5}	38×10^{-5}

¹Fiducial registration errors (FRE, in mm) estimated using selected fiducial markers not used in the FEM model calculation for PET-MR coregistration. A total of 27 identifiable markers were available.

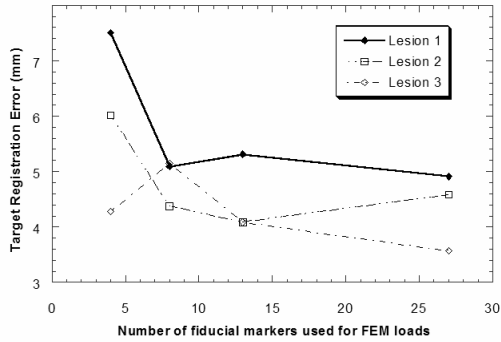


Fig. 5. Dependence of target registration error (TRE) on number of fiducial markers used in steady-state FEM model. Data are shown for three representative “lesions” of the six (see locations, by number, in Fig. 2).

Patient Studies

Patient 1

We coregistered and fused prone high-resolution (HiRes) 3D fast field echo (FFE) MRI with F-18-FDG prone PET. Our method (Fig. 6a) yielded improved coregistration of the enhanced metabolic activity region revealed by PET with the well-defined lesion demonstrated by HiRes MRI (Fig. 6c), as compared to pure rigid registration (Fig. 6b). It is possible now to determine which part of the lesion is metabolically hyperactive.

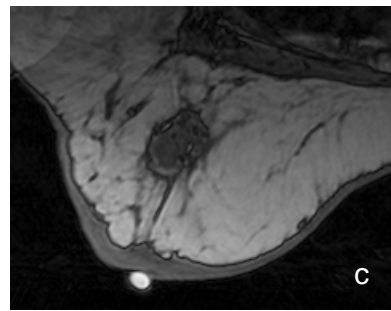
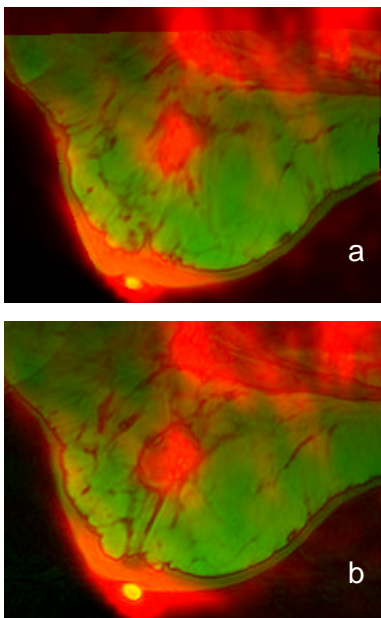
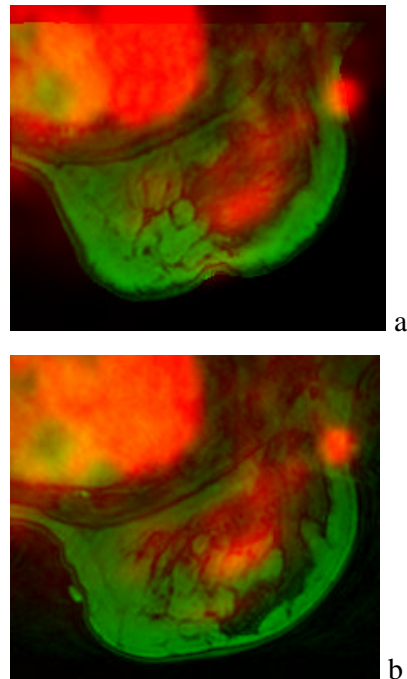


Fig. 6. Coregistered and fused TA images of patient #1, slice 120: red channel-PET, green channel-high resolution MRI, pixel size 0.7 mm, **a.** after SSHT FEM registration; **b.** after rigid registration, **c.** MRI only.

Patient 2

We coregistered and fused prone high-resolution (HiRes) 3D FFE MRI (not shown) and dynamic gradient recalled echo (GRE) MRI with F-18-FDG prone PET and post-Gd1 dynamic image series. Our method (Fig. 7a) yielded improved coregistration of the enhanced metabolic activity region revealed by PET with the enhanced wash-in region demonstrated by differential dynamic image series (preGd-postGd1) MRI (Fig. 7c), as compared to rigid only registration (Fig. 7b). It is possible now to determine spatial correlation of metabolically active lesions visible in PET and MRI.



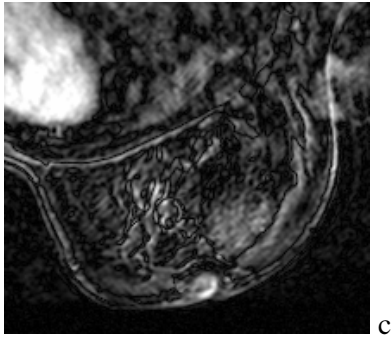


Fig. 7. Coregistered and fused images of patient #2, slice 147: red channel-PET, green channel-post-Gd1. Pixel size 0.7 mm. **a.** after SSHT FEM registration; **b.** after rigid registration only; **c.** registered differential dynamic image series (preGd-Gd1) using GRE sequence.

DISCUSSION AND CONCLUSIONS

The SSHT deformable FEM-based breast model performs well for multimodality elastic breast phantom image co-registration. This co-registration procedure requires external fiducial markers that have to surround the suspicious lesion, and it requires very careful breast positioning to prevent changes in the internal stress conditions between different modalities. We tested our model on a small number of patients imaged with fiducial skin markers using PET and MRI. For lesions that were visible in both PET and MRI, the target registration error is less than the width of two PET voxels for intermodal coregistration. Subtraction of the motion-corrected post-injection images from the pre-injection image revealed the true spatial distribution of the contrast material.

REFERENCES

1. American Cancer Society, *Cancer Facts and Figures*, <http://www.cancer.org>.
2. C. J. Baines, *Natl. J. Cancer Inst.*, **90**, 875, (1998).
3. *ANSYS Theory Reference*, 11th Edition, SAS IP Inc. (1999).
4. D. Pepper and J. C. Heinrich *The Finite Element Method: Basic Concepts and Applications* Hemisphere Publishing, 1992.